Post-launch calibration of Ocean Colour Monitor 2 using Kavaratti CAL-VAL site observations

K. N. Babu, A. K. Shukla, V. N. Sridhar, Ajai, B. Damiri and F. J. O. Reyes

Oceansat-2 mission is envisaged to provide continuity of services for the operational users of Ocean Colour Monitor (OCM) data as well as enhance the application potential in other areas. It was successfully launched by PSLV-C14 flight on 23 September 2009 from Shriharikota launch pad. It carried three payload instruments, viz. OCM 2, a Ku-band scatterometer (OSCAT) and a Radio Occultation Sounder for Atmosphere (ROSA) which has been developed by the Italian Space Agency. A controlled calibration and validation site is envisaged in southeast Arabian Sea to monitor the OCM 2 sensor stability owing to its post-launch performance and ageing-related problems in orbit. This site measures hyper-spectral optical radiances (both in air and underwater), meteorological parameters and CIMEL 318 sun-photometer for sun and sky radiation in automated mode. All these datasets are received from the site via satellite communication. These measurements are analysed along with top-of-the-atmosphere (TOA) radiance measured by OCM 2 sensor. The OCM 2 sensor performance is monitored against the radiance computed at TOA through a forward radiative transfer model for the period spanning from 23 September 2009 to 24 April 2010.

Ocean colour satellite provides the scientific community a means of studying the biosphere on temporal and spatial scales unattainable using conventional *in situ* sampling platforms. This was aptly demonstrated by the proof-of-concept Coastal Zone Color Scanner sensor[1,2]. Drawing on its successful legacy, a number of advanced ocean colour satellite instruments were launched in the past decades. These sensors measure the spectra of reflected sunlight emanating upward from the top of the Earth's atmosphere at visible and near-infrared wavebands. The satellite sensor observed radiance over the clear sky ocean comprises various components, i.e. scattering by air molecules and aerosol particles in the atmosphere, those emerged from the ocean body and those reflected by the ocean surface. Among them, only the radiance from the ocean body, or the 'water-leaving radiance' L_w, contains information about the quality of the ocean surface water. The spectral water-leaving radiance, $L_w(\lambda)$, the light backscattered out of the ocean, is obtained by removing the contribution of the atmosphere from the total signal[3]. The $L_w(\lambda)$ is used to estimate a number of geophysical data parameters through the application of secondary bio-optical algorithms[4] and subsequently in higher-level parameters, as is the case for marine primary production[5], global carbon cycle research[6], assimilation into global circulation models, fisheries regulation, and coastal zone monitoring and management[7].

Before they become useful for such areas of application, the top-of-the-atmosphere (TOA) radiance observations from these satellite sensors (i.e. the radiance backscattered by the Earth's surface and atmosphere recorded in several finite spectral bands) have to be properly validated. Then the geophysical parameters that are subsequently derived from these TOA observations through a series of algorithms have to be validated against so-called sea-truth data. The validation of data from several sensors against a unique set of *in situ* data is also a mandatory step before they can be merged, which is nowadays one of the major goals of the international ocean colour community[8]. Satellite sensors that make quantitative ocean colour radiometric measurements require a more exacting calibration than do land sensors because of the small signal of the ocean relative to the atmosphere. As several spectral bands are involved in bio-optical algorithms to estimate geophysical data products from these radiances, absolute calibration errors can get magnified[9].

The post-launch Ocean Colour Monitor (OCM) 2 sensor performance has been assessed using Kavaratti CAL-VAL site data and vicarious gains for its eight spectral bands have been computed. The results presented here are generated from ten very clear days, synchronous measurements with OCM 2 passes over the site during September 2009 to April 2010. The present work describes an approximate model proposed for the estimation of OCM 2 sensor radiance along the sun-sensor geometry based on field measurements and the vicarious calibration gain coefficients, obtained from vicarious calibration exercises based on the proposed forward radiative transfer equation model and *in situ* measurements.

Data and methodology

Satellite data

OCM 2 is an 8-band multi-spectral camera operating in the visible–near-infrared spectral range. It provides an instantaneous geometric field of view of 360 m and ground sampling distance of 236 m (along track) covering a swath width of 1420 km. Each lens assembly contains a linear array charge coupled device (CCD) of 6000 pixels in the focal plane and the spectral band-pass filter in front of the CCD. Out of 6000 pixels, 3730 pixels in the centre are used to cover the image field. To avoid sun glint due to specular reflection from the ocean surface, there is provision to tilt the OCM 2 by $\pm 20°$ in the along-track direction. On-board calibration scheme using light-emitting diodes mounted near each CCD is incorporated to study long-term stability of the radiometric performance[10]. The major specifications of OCM 2 are given in Table 1.

In situ data

Field data for vicarious calibration exercise have been collected at the CAL-

VAL site (72.27°E; 10.61°N). The site is characterized by presence of Case-1 water[11]. The optical buoy has been collecting measurements of up-welling and down-welling radiance using HydroRad 2 hyperspectral radiometer at this clear-water site since 2008 (removed during southwest monsoon season). These radiometers provide 1 nm spectral readings from 350 to 850 nm and thus match the spectral response of each of the eight OCM 2 bands. The L_w processing procedure adheres to the community-vetted ocean optics protocols[12]. According to the protocol, the shallowest observations of upwelled spectral radiances are propagated upward to just beneath the sea surface by calculating the upwelled spectral radiance attenuation coefficient and then the radiance loss between the surface and depth z. The subsurface upwelled radiances are then transmitted through the sea surface. Thus the spectral water leaving radiance $L_w(\lambda)$ is given as

$$L_w(\lambda) = L_u(z_1) \times \exp\left(\ln\left[\frac{L_u(z_1,\lambda)}{L_u(z_2,\lambda)}\right]\frac{1}{z_2 - z_1} * z_1\right) * \frac{t}{n^2}, \quad (1)$$

where $L_u(z_1)$ and $L_u(z_2)$ are the subsurface upwelling radiances respectively, obtained at depths z_1 and z_2, t is the air–sea transmission coefficient and n is the refractive index of sea water. These high-resolution spectra are then convolved with the OCM 2 spectral response to form the band-averaged L_w, since they are assumed to be the most accurate values for comparison with the satellite.

Table 1. Major specifications of Ocean Colour Monitor (OCM) 2 (after Venkata Rao[10])

Parameters	Specifications
GIFOV (km)	0.360 × 0.236
Swath (km)	1420
Repetivity (days)	2
Local time of pass	12 noon ± 10 min
Altitude (km)	720
Along-track steering	± 20°
Spectral bands (nm)	402–422
	433–453
	480–500
	500–520
	545–565
	610–630
	725–755
	845–880
Quantization	12 bits

Direct sun irradiance and sky radiance data are also measured with the CE-318 sun photometer and inverted to obtain the aerosol optical depth (AOD) and single scattering albedo (SSA)[13–16]. The AOD datasets are screened from cloud contamination following Smirnov *et al.*[17]. Using second-order polynomial/spline fitting method and OCM 2 spectral response function, the AOD and SSA at OCM 2 channels are computed.

Vicarious calibration

Diversity of the vicarious calibration requirement suggests a variety of organizational schemes for executing the tasks involved. The formalism adopted was derived from the equation governing the basic ocean colour sensor measurement, the radiative transfer equation for the radiance observed in orbit. In practice, the vicarious calibration equates the TOA radiance over the ocean surface with that of ocean colour sensor measurement. The radiance received by a sensor at TOA in a spectral band centred at a wavelength λ, $L_t(\lambda)$, can be divided into the following components: $L_{\text{path}}(\lambda)$ the radiance generated along the optical path by scattering in the atmosphere and by specular reflection of atmospherically scattered light (skylight) from the sea surface, $L_g(\lambda)$ the contribution arising from specular reflection of direct sunlight from the sea surface (sun glitter), $L_{wc}(\lambda)$ the contribution arising from sunlight and skylight reflecting from individual whitecaps on the sea surface[18,19], and $L_w(\lambda)$ the measured water-leaving radiance, that is

$$L_t(\lambda) = L_{\text{path}}(\lambda) + T(\lambda)L_g(\lambda) + T(\lambda)L_{wc}(\lambda) + t(\lambda)L_w(\lambda). \quad (2)$$

In general, $L_{\text{path}}(\lambda)$ can be approximated rather than considering several components. We considered single-scattering approximation proposed by CZCS algorithm[20]. In this approximation the path radiance reduces to

$$L_{\text{path}}(\lambda) = L_r(\lambda) + L_{as}(\lambda), \quad (3)$$

where $L_r(\lambda)$ and $L_{as}(\lambda)$ represent the radiance associated with Rayleigh scattering[21] and singly-scattered aerosol scattering. The $t(\lambda)$ term accounts for diffuse transmittance of the atmosphere[1] along the sensor view path from the surface to the satellite. $T(\lambda)$ is the direct transmittance of the atmosphere. Areas where the sun glint is significant can be predicted and avoided; residual glint outside the main region of glint contamination can be removed[22]. Hence eq. (2) can be written as

$$L_t(\lambda) = L_{\text{path}}(\lambda) + T(\lambda)L_{wc}(\lambda) + t(\lambda)L_w(\lambda). \quad (4)$$

The phase function due to aerosol scattering is approximated by a two-term Heyney–Greenstein phase function for the marine aerosols[23].

The resulting $L_t(\lambda)$ is compared to the satellite-measured $L_t(\lambda)$ and a gain coefficient, g_λ, is derived that would force agreement of the measured $L_t^m(\lambda)$ and the vicarious $L_t^v(\lambda)$

$$g_\lambda = \frac{L_t^{\text{vicarious}}(\lambda)}{L_t^{\text{measured}}(\lambda)}, \quad (5)$$

The final g_λ is determined as

$$\left[\sum_{j=1}^{N} g_\lambda(j)\right] \Big/ N. \quad (6)$$

where the index j refers to the individual g_λ values and N is the number of calibration points.

For each *in situ* record, the corresponding local area coverage resolution satellite data file was identified. A nominal 1° × 1° box centred on the *in situ* location was extracted from the full satellite file. Satellite data are navigated to identify the pixel that corresponds with each *in situ* location. Here the *in situ* data are collected exactly when the satellite views the site. Restricting the box size to odd dimensions is required to identify the location of interest at the centre of the box. We desire a small sampling box as we assume that as box size increases, geophysical variability may be introduced in violation of our requirement of homogeneity. We ultimately selected a 5 × 5 pixel box to limit the inaccuracy posed by geophysical variability, errors in navigation, while maintaining a reasonably small sampling area.

Sensitivity study

A sensitivity study is performed to see the model behaviour with varying input

parameter. The parameters considered for this study are AOD, water-leaving radiance and wind speed. All these parameters are varied up to 10% from its actual measured values.

Sensitivity on aerosol optical depth

The percentage change in modelled OCM 2 TOA radiance against the percentage change in AOD is shown in Figure 1. Among all the eight channels of OCM 2 sensor, the detected radiance has high sensitivity for the bands 7 and 8 for varying atmosphere AOD loading. For other channels the percentage change in modelled TOA radiance is very less. For maximum of ± 10% change in AOD, the TOA changes to ± 4%.

Sensitivity on water-leaving radiance

The measured L_w is the input in forward radiative transfer equation (RTE) model. The sensitivity study of this parameter on model output is carried out by varying the input to maximum of 10%. The middle four OCM 2 (490, 510, 555, 620 nm) channels have maximum (2.2%) sensitivity with varying L_w (10%). The other four channels were found to be moderate to less sensitive for the varying water-leaving radiance. The sensitivity plot is shown in Figure 2.

Sensitivity on wind speed

The sensitivity plot of modelled TOA with varying wind speed is shown in Figure 3. Wind speed has an impact on TOA modelling for near-infrared channels and the model is less sensitive to variation in wind speed for visible channels.

Results and discussion

The OCM 2 level L1B products from National Remote Sensing Centre (NRSC), Hyderabad were used. The OCM 2 radiances for all spectral bands are scaled down using the updated calibration coefficients provided by the OCM 2 Payload Group[24]. Following Franz *et al.*[25], the exclusion criteria applied to the data as the baseline for this study include: chlorophyll-*a* concentration of less than 0.25 mg/m^3, AOD (870) of less than or equal to 0.21, solar zenith angle of less than 70°, and sensor zenith angle of less than 56°. We excluded data which are having band 8 (865 nm) radiance greater than 1 μW/cm^2/sr/nm. Data are also excluded which are contaminated by stray light, and sun glint (through visual observation). We also excluded extreme variation between pixels in the defined

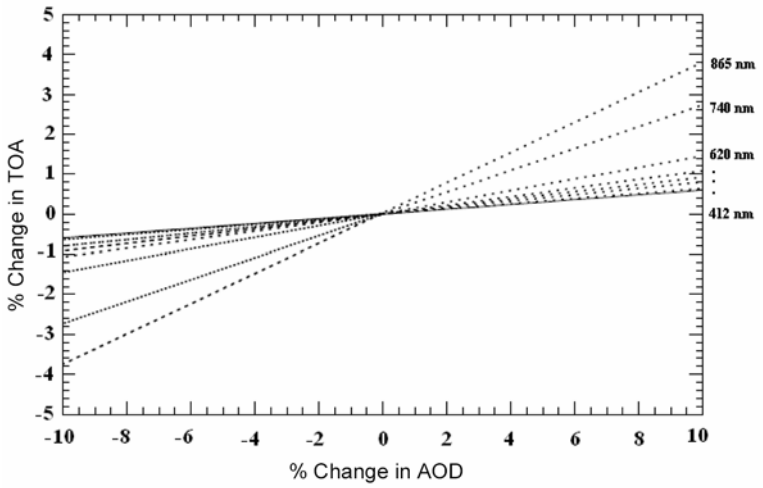

Figure 1. Sensitivity of modelled top-of-the-atmosphere (TOA) radiance (μW/cm^2/sr/nm) against aerosol optical depth (AOD).

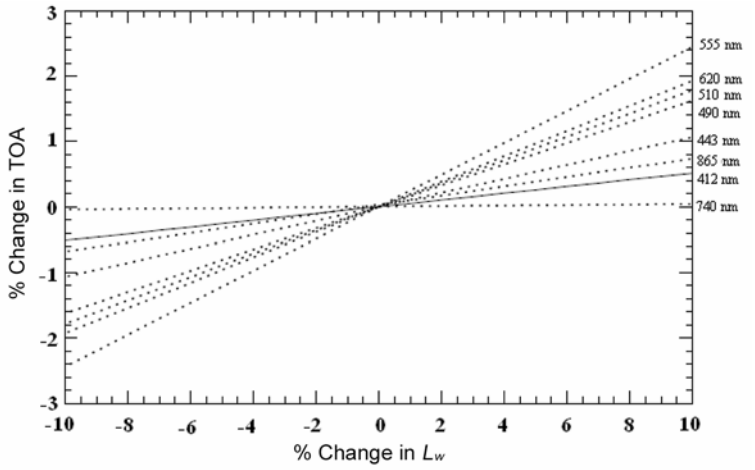

Figure 2. Sensitivity of modelled TOA radiance (μW/cm^2/sr/nm) against the L_w the water leaving radiance (μW/cm^2/sr/nm).

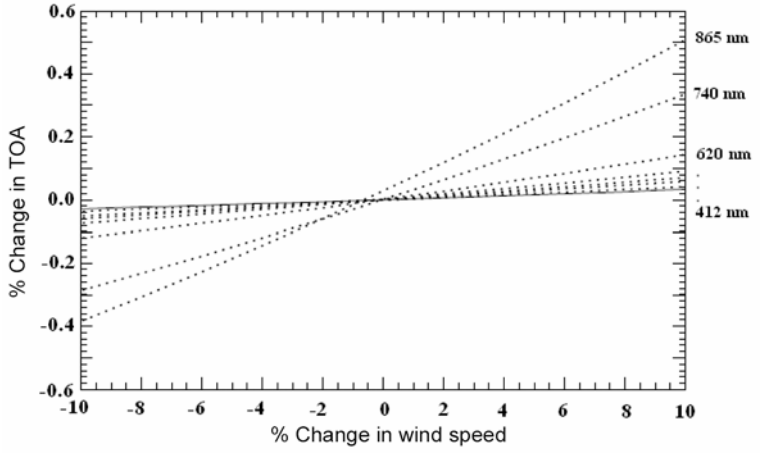

Figure 3. Sensitivity of modelled TOA radiance (μW/cm^2/sr/nm) against wind speed (m/s).

Table 2. OCM 2 top-of-the-atmosphere (TOA) radiance at 865 nm (μW/cm^2/sr/nm), standard deviation of TOA radiance at 865 and measured aerosol optical depth (AOD) at 870 nm

Date	Mean (5 × 5) pixel	SD (5 × 5) pixel	*In situ* AOD (870 nm)
19/11/09	0.30	3.13e-3	0.07
15/12/09	0.51	3.19e-2	0.21
18/01/10	0.40	4.64e-3	0.15
20/01/10	0.40	4.71e-3	0.16
24/01/10	0.43	8.63e-2	0.11
28/01/10	0.55	5.40e-3	0.19
03/02/10	0.41	1.40e-2	0.17
05/02/10	0.47	5.72e-3	0.21
09/02/10	0.42	4.64e-3	0.11
17/02/10	0.48	1.13e-2	0.16

Table 3. Statistics of OCM 2 and computed radiances for nine clear days over Kavaratti (KVT) site

Band	Mean modelled KVT TOA radiance (μW/cm^2/sr/nm)	Mean measured OCM 2-TOA radiance before correction (μW/cm^2/sr/nm)	Vicarious gain = KVT/OCM 2	Percentage of relative difference
1	8.9 ± 0.4	8.5 ± 0.6	1.05	–4.85
2	7.6 ± 0.4	7.6 ± 0.6	1.00	–0.11
3	5.7 ± 0.4	6.0 ± 0.4	0.96	4.57
4	4.5 ± 0.4	4.4 ± 0.3	1.02	–2.08
5	3.3 ± 0.4	3.2 ± 0.2	1.04	–3.89
6	2.0 ± 0.2	1.8 ± 0.2	1.11	–10.14
7	0.8 ± 0.1	0.7 ± 0.1	1.06	–4.55
8	0.4 ± 0.1	0.4 ± 0.1	0.92	9.72

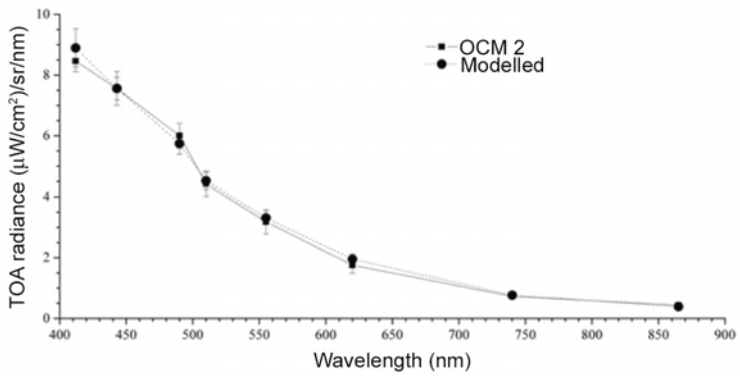

Figure 4. The uncorrected Ocean Colour Monitor (OCM) 2 TOA and modelled TOA radiances for nine days.

box (coefficient of variance greater than 0.1). These pixels typically represent frontal regions or other anomalies (e.g. cloud edges), which makes the calibration/validation results questionable[26]. Approximately 90% of the potential calibration dates were eliminated due to lack of sufficient valid satellite pixels, primarily due to cloud cover, high aerosol optical thickness and spatial heterogeneity. Based on these conditions we came out with 10 very clear dates for the analysis over Kavaratti site during this season. Table 2 shows the dates selected for the analysis with additional information. Here OCM 2 TOA radiance is an average value rather than individual. The filtered mean value from 5 × 5 pixel window centred on the geo-location of optical buoy is taken for the analysis.

Filter mean

$$= \frac{\sum_i (1.5 * \sigma - \overline{X}) < X_i < (1.5 * \sigma + \overline{X})}{N}, \quad (7)$$

where $\overline{X}$ is the unfiltered mean value, σ is the standard deviation of the unfiltered data and N is the number of values within $\pm 1.5 * \sigma$.

The vicarious calibration exercise was performed with a subset of the data whose dates are listed in Table 2.

Following the methodology as explained earlier, OCM 2 TOA sensor radiance is computed from the measurements done at Kavaratti CAL-VAL site through forward atmospheric radiative transfer approach. Kavaratti CAL-VAL site-measured parameters (from the optical buoy, met-buoy and sun photometer) are used in this model. The L_w is taken from optical buoy observations. The atmospheric pressure, air temperature, water temperature and wind speed are taken from the met-buoy observations. The single-scattering albedo (ω) and aerosol optical thickness is obtained from the sun photometric observation. The sun and sensor geometry over Kavaratti site is taken from OCM 2 level L1B product. Table 3 shows the statistics between OCM 2 modelled and measured TOA radiances. Differences were noticed between OCM 2 measured radiance and modelled OCM 2 radiance over Kavaratti CAL-VAL site (Figure 4). Based on the results, vicarious gain coefficients are computed between modelled OCM 2 and measured OCM 2 TOA radiances for all eight spectral bands. These results are based on data of nine days out of the total ten days of data as collected by OCM 2.

The largest uncertainties in the vicarious calibration process are not associated with the atmospheric correction process or the *in situ* instruments, but rather with the natural environment[27]. The collection of coincident measurements of atmospheric properties, such as aerosol optical thickness, was intended to provide a means for reducing the uncertainty in the selection of the aerosol models used by the atmospheric correction code in the vicarious calibration process. To estimate first-order uncertainties in the vicarious calibration, we incorporated vicarious gain coefficients to correct the TOA radiance of 17 February 2010 OCM 2 radiance, which is not used in the computation. Table 4 shows the results of this calculation. Here, the corrected OCM 2 measured radiances closely match the modelled TOA radiances (Figure 5).

The satellite to *in situ* mean ratios and percentage of relative difference approach

Table 4. Verification of KVT vicarious gain on 17 February 2010 OCM 2-TOA radiance

Band	Modelled KVT TOA radiance ($\mu W/cm^2/sr/nm$)	Measured OCM 2 TOA radiance ($\mu W/cm^2/sr/nm$)	Modified OCM 2 TOA radiance ($\mu W/cm^2/sr/nm$)	Percentage of relative difference	Modelled/ modified
1	8.63	8.33	8.74	1.30	0.99
2	7.38	7.46	7.46	1.13	0.99
3	5.60	6.01	5.77	2.92	0.97
4	4.38	4.39	4.48	2.31	0.98
5	3.20	3.22	3.35	4.57	0.96
6	1.87	1.81	2.01	7.05	0.93
7	0.75	0.77	0.82	9.02	0.92
8	0.42	0.48	0.44	3.65	0.96

Table 5. Final vicarious gain coefficient

Band	1	2	3	4	5	6	7	8
Gain	1.04	1.00	0.95	1.02	1.04	1.10	1.05	0.91

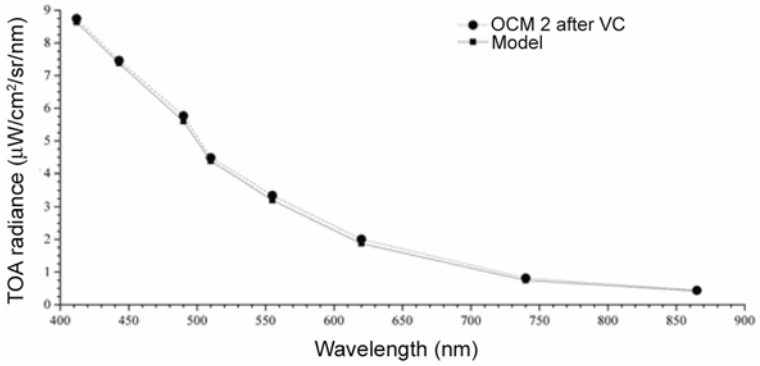

Figure 5. The 17 February 2010 results for OCM 2 channels.

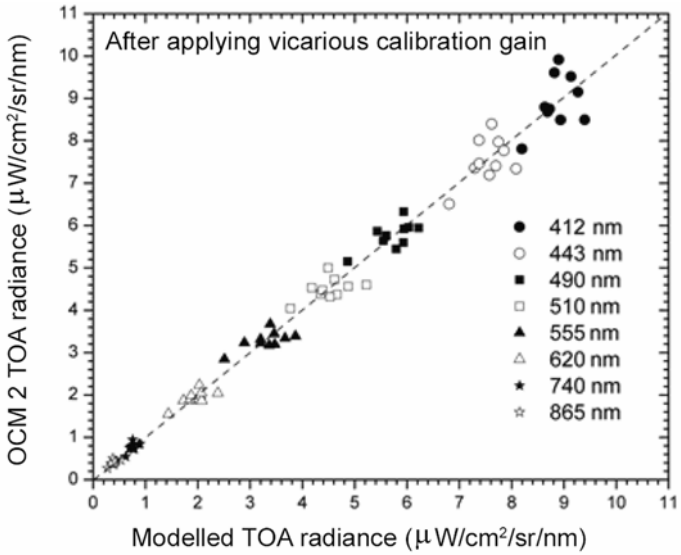

Figure 6. The modelled and OCM 2 TOA radiance after applying Kavaratti vicarious calibration gain.

unity and zero respectively, which demonstrates that the calibration was executed properly. The results on 17 February 2010, indicate near unity in ratio between modelled TOA radiance and modified OCM 2 TOA radiance and the percentage of relative difference less than 4 for the first five bands. The band 6 (620 nm) percentage of relative difference increases to 10.14 and for band 8 (865 nm) the percentage of relative difference is close to 9.72. After verifying

the approach of modelling TOA radiance using Kavaratti observations/measureents, we took the mean vicarious calibration gain coefficients from all ten days. The mean values for OCM 2 bands are given in Table 5. The scatter of modelled TOA radiance and modified OCM 2 TOA radiance (after applying vicarious calibration gain coefficient) is shown in Figure 6. The relative percentage difference between the modelled radiance and OCM 2 measured radiances is well within 10%. The comparatively poor result for the 620 nm band is not unexpected, as the attenuation of pure sea water at wavelengths longer than 620 nm leads to water-leaving radiances close to zero in clear water. The radiance ratios are therefore extremely sensitive to small differences between the calculations and satellite retrievals, and the negligible dynamic range makes regression correlations meaningless.

Conclusion

The path radiance estimated using field measurements has shown the capability of providing satisfactory results in producing TOA radiance over Kavaratti site. The relative percentage difference between the modelled radiance and OCM 2 measured radiances is well within 10%. For higher wavelengths, the radiance ratios are therefore extremely sensitive to small differences between the calculations and satellite retrievals and the negligible dynamic range makes regression correlations meaningless.

1. Gordon, H. R., Clark, D. K., Brown, J. W., Brown, O. B., Evans, R. H. and Broenkow, W. W., *Appl. Opt.*, 1983, **22**, 20–36.
2. Hovis, W. A. *et al.*, *Science*, 1980, **210**, 60–63.
3. Gordon, H. R. and Wang, M., *Appl. Opt*., 1994, **33**, 443–452.
4. O'Reilly, J. E. *et al.*, *J. Geophys. Res*., 1998, **103**, 24937–24954.
5. Behrenfeld, M. J. and Falkowski, P. G., *Limnol. Oceanogr.*, 1997, **42**, 1479–1491.
6. McClain, C. R., Hooker, S. B., Feldman, G. C. and Bontempi, P., *EOS, Trans. Am. Geophys. Union*, 2006, **87**, 337–343.
7. Sathyendranath, S. (ed.), Report of the International Ocean Colour Coordinating Group, IOCCG, Dartmouth, Canada, 2000, vol. 3, p. 140.
8. Antoine, D. (ed.), Report of the International Ocean Colour Coordinating Group, IOCCG, Dartmouth, Canada, 2004, vol. 4, p. 88.
9. Richard, P. S. and Werdell, P. J., *Opt. Express*, 2009, **18**, 401.
10. Venkata Rao, M., OceanSat-2 mission and applications, Dept of Space, Government of India, Bangalore, 2010, NNRMS (B)-34, pp. 1–6.
11. Babu, K. N., Shukla, A. K., Matondkar, S. G. P., Singh, S. K. and Sawant, S., *J. Mar. Geodesy*, 2009, **32**, 345–354.
12. Mueller, J. L. *et al.*, NASA Technical Memorandum 2003-211621/Rev4, NASA Goddard Space Flight Center, Greenbelt, MD, 2003, vol. III, p. 78.
13. Nakajima, T., Tamaka, M. and Yamauchi, T., *Appl. Opt.*, 1983, **22**, 2951–2959.
14. Nakajima, T., Tonna, G., Rao, R., Boi, P., Kaufman, Y. and Holben, B., *Appl. Opt.*, 1996, **35**, 2672–2686.
15. Lyamani, H., Olmo, F. J., Alcántara, A. and Alados-Arboledas, L., *Atmos. Environ.*, 2006, **40**, 6465–6476.
16. Olmo, F. J., Quirantes, A., Alcántara, A., Lyamani, H. and Alados-Arboledas, L., *J. Quant. Spectrosc. Radiat. Transfer*, 2006, **100**, 305–314.
17. Smirnov, A. *et al.*, *Remote Sensing Environ*., 2000, **73**, 337–348.
18. Monahan, E. C. and O'Muircheartaigh, I. G. O., *Int. J. Remote Sensing*, 1986, **7**, 627–642.
19. Koepke, P., *Appl. Opt.*, 1984, **23**, 1816–1824.
20. Gordon, H. R., *J. Geophys. Res. D*, 1997, **102**, 17081–17106.
21. Hansen, J. E. and Travis, L. D., *Space Sci. Rev.*, 1974, **16**, 527.
22. Wang, M. and Bailey, S., In NASA Technical Memorandum 1999-206892 9 (eds Hooker, S. B. and Firestone, E. R.), NASA Goddard Space Flight Centre, Greenbelt, MD, 2000.
23. Sturm, B., In *Remote Sensing in Meteorology, Oceanography and Hydrology* (ed. Cracknell, A. P.), Ellis Horwood Ltd, Chichester, 1980, pp. 163–197.
24. SSD/EOSG, Note on updated calibration coefficients for OCM instrument of Oceansat-2 based on FEL lamp-and-diffuser based radiance scale (SAC/OSG/SSD/2962010/23A), 2010.
25. Franz, B. A., Bailey, S. W., Werdell, P. J. and McClain, *Appl. Opt*., 2007, **46**, 5068–5082.
26. Kilpatrick, K. A., Podesta, G. P. and Evans, R., *J. Geophys. Res.*, 2001, **106**, 9179–9198.
27. Bailey, S. W., Hooker, S. B., Antoine, D., Bryan, A. F. and Werdell, P. J., *Appl. Opt.*, 2008, **27**, 2035–2045.

ACKNOWLEDGEMENTS. We thank Dr R. R. Navalgund, Director, Space Applications Centre (SAC), Ahmedabad for encouragement and suggestions. The valuable guidance from Dr A. S. Kirankumar, Associate Director, SAC and useful suggestions from Dr J. S. Parihar, Deputy Director, EPSA and Dr A. Sarkar, Project Director, Oceansat 2 utilization programme are acknowledged. We thank NRSC, Hyderabad NDC team for providing the OCM 2 data. Calibration coefficients for OCM 2 were provided by the OCM 2 Payload Group. We also acknowledge the Atmospheric Physics Group, University of Granada, Spain, CIMEL Electronique, France and Prof. Nakajima for providing the inversion code.

Received 17 May 2012; revised accepted 9 November 2012

K. N. Babu, A. K. Shukla, V. N. Sridhar and Ajai are in the Marine, Geo and Planetary Sciences Group, Space Applications Centre (ISRO), Ahmedabad 380 015, India; B. Damiri is in the Cimel Electronique, 172 Rue De Charonne, 75011 Paris, France; F. J. O. Reyes is in the Departamento de Física Aplicada, Universidad de Granada, Fuentenueva s/n, 18071-Granada, Spain.*
**e-mail: kn_babu@sac.isro.gov.in*